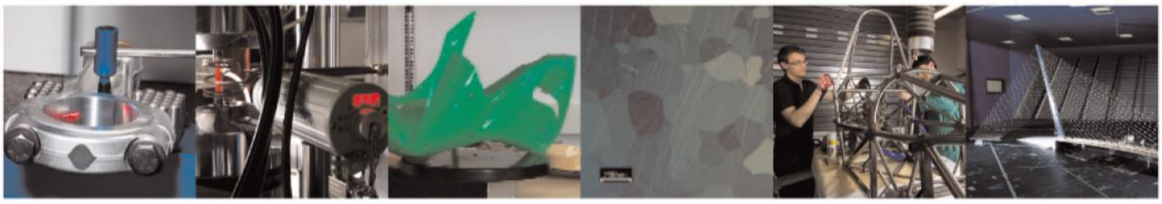

A Lamb Waves Based Statistical Approach To Structural Health Monitoring Of Carbon Fibre Reinforced Polymer Composites

Michele CARBONI, Andrea GIANNEO, Marco GIGLIO

This is a post-peer-review, pre-copyedit version of an article published in Ultrasonics. The final authenticated version is available online at: http://dx.doi.org/10.1016/j.ultras.2015.02.011

DIPARTIMENTO DI MECCANICA ■ POLITECNICO DI MILANO
via G. La Masa, 1 ■ 20156 Milano ■ EMAIL (PEC): pecmecc@cert.polimi.it
http://www.mecc.polimi.it
Rev. 0

A LAMB WAVES BASED STATISTICAL APPROACH TO STRUCTURAL HEALTH MONITORING OF CARBON FIBRE REINFORCED POLYMER COMPOSITES

Michele CARBONI*, Andrea GIANNEO, Marco GIGLIO

Department of Mechanical Engineering – Politecnico di Milano

Via La Masa 1, 20156 Milano, Italy

ABSTRACT

The research investigates a Lamb-Wave based structural health monitoring approach matching an out-of-phase actuation of a pair of piezoceramic transducers at low frequency. The target is a typical quasi-isotropic carbon fibre reinforced polymer aeronautical laminate subjected to artificial, via Teflon Patches, and natural, via suitable low velocity drop weight impact tests, delaminations. The performance and main influencing factors of such an approach are studied through a Design of Experiment statistical method, considering both Pulse Echo and Pitch Catch configurations of PZT sensors. Results show that some factors and their interactions can effectively influence the detection of a delamination-like damage.

Key words: Carbon Fibre Reinforced Polymer Composite, Ultrasonic Lamb Waves, Structural Health Monitoring, Barely Visible Impact Damage, Design of Experiments, Analysis of Variance

1. Introduction

Carbon Fibre Reinforced Polymer (CFRP) composites have been developed since the '60s [1] and allow [2] the design of resistant and innovative light weight primary structures, replacing traditional metallic materials, due to their high strength–weight and moduli-weight ratios, excellent fatigue strength as well as fatigue damage tolerance. Another advantage is their non-corroding behaviour. However, their intensive structural use remains almost limited due to, among other factors, several peculiar damage mechanisms,

* Corresponding author: Tel.: +39-02-23998253, Fax: +39-02-23998202, E-mail: michele.carboni@polimi.it.

which are able to degrade quickly the mechanical properties and strength [2]. An interesting example, analysed later on in this research, is the “barely visible impact damage” (BVID) [3] likely occurring to in-service structures, because, in spite of negligible external indications of damage, it can cause [4, 5] a complex pattern of matrix cracks, fibre breakages and a significant amount of delamination. Therefore, a dramatic loss of residual structure’s strength and fatigue life is observed [5].

In order to detect damages like BVID and prevent catastrophic failures, structures are periodically inspected, at planned maintenance service interruptions, by means of non-destructive testing (NDT). The main NDT techniques applied to composite materials and structures are: visual testing, eddy currents testing, ultrasonic testing, vibration analysis, radiography and tomography. A good state-of-the-art on this subject can be found in [6, 7]. Unfortunately, the NDT common practise, especially for safety components, results in high maintenance costs. In particular, in spite of the high level of reliability nowadays reached, maintenance and repairs represent about one quarter of the operational costs of a commercial aircraft; moreover, a significant amount of civil and military aircrafts has, today, exceeded its design lifetime [8, 9]. Therefore, an increasing solution, proposed in the literature [10], is the application of Structural Health Monitoring (SHM) approaches which, in the aeronautical field, have shown the potentiality to significantly decrease [8, 9] the overall costs of traditional NDT, since the planned maintenance service interruptions can be substituted by condition-based maintenance. More importantly, SHM can prevent catastrophic disasters by identifying and monitoring developing defects before their degeneration into a failure, with significant improvements in reliability. Nowadays, the applied SHM techniques are, in general, based onto different physical phenomena [10]: dynamic modal data, electro-mechanical impedance, static parameters (displacement field, strain gauges, Bragg fibres, …), acoustic emission (AE) or elastic waves. Those capitalising on modal data are generally [11] less sensitive to damage until it reaches a threshold value able to influence the global dynamic response of the material/component, whereas electro-mechanical impedance and static parameters are relatively insensible [11] to damage developing far away from the transducers. AE is generated by developing damages in terms of elastic waves and it is an effective way of localization via triangulation and of evaluation of the failure behaviour of composite materials [12]. However, it is a passive technique, so it requires loaded components and it is prone to environmental noise contamination. Furthermore, most of the aforementioned techniques employ bulky transducers (AE), require point scanning (strain gauges, Bragg fibres, electro-mechanical impedance, …), are expensive (Bragg fibres) or quite insensitive until a threshold value is reached (dynamic modal data).

This research work investigates ultrasonic techniques based on Lamb waves, which were firstly described by Lamb [13] for homogeneous isotropic materials and have been studied over the last few decades [14-19] as a very attractive SHM method. Compared to other SHM approaches, those capitalizing on Lamb waves can offer faster and more cost-effective evaluation of various types of damage. Lamb waves, i.e. elastic thickness waves, can reach relatively long distances (a few meters), even within materials with high attenuation ratios, allowing to cover wide inspection areas using few transducers. Being highly susceptible to both surface and embedded structural damage, they were widely used to develop damage identification approaches for delaminations, holes, cracks/notches, corrosion, degradation of lap joints; details are summarized in [20]. However, because multiple wave modes are synchronously involved and overlap each other (at least, two fundamental modes are typically present) and because of their dispersive behavior, a captured Lamb wave signal is often complex to be interpreted. Consequently, many efforts are available in the literature [11, 21-22] to isolate a “pure” single propagation mode. All of them are mainly based onto the rationale that a desired wave mode can be enhanced while the others deleted or minimized by generating mutual interactions of various Lamb wave modes using a series of appropriately located PZT transducers. This approach, as reported by Su et al. [11], is often termed “multi-sensor mode tuning technique”.

Another difficulty in the application of Lamb waves consists in the fact that, propagating at fast velocities, wave packets reflected by structural boundaries or geometrical discontinuities can easily mask damage-scattered wave packets. Moreover, Lamb waves are prone to contamination from a variety of interference sources including high-frequency ambient noise, low-frequency structural vibration, temperature fluctuation, inhomogeneity and anisotropy of materials.

In the present paper, the propagation phenomenon of Lamb waves is firstly studied, with the aim to set up a “single propagation mode” approach, considering a quasi-isotropic CFRP laminate composed of 17 unidirectional (UD) pre-preg SAATI EH-550/T800S laminas with stacking sequence [0/+45/0/-45/90/-

45/0/+45/90]$_s$ [23]. The fibre (T800S) considered in the CFRP laminate is the reference one for the primary structure of the Airbus A380 aircraft, but no comprehensive information could be retrieved, from the literature, about the elastic and ultrasonic properties of the chosen carbon-fibre composite system. For this reason, the study starts with the experimental characterization of the elastic properties of the material and with the determination of its dispersive behaviour through an experimentally validated Semi-Analytical Finite Element (SAFE) approach.

Then, the influence of the main key factors acting on the interaction and scattering of the diagnostic signal with artificial and natural BVID damages is analysed through the “Design of Experiments” (DOE) and “Analysis of Variance” (ANOVA) statistical approaches [24]. These methodologies were developed and are wide spread in the manufacturing field to optimize technological parameters during production. For what the authors know, no application to SHM has been tried yet. Moreover, it is worth remarking both “Pulse-Echo” and “Pitch-Catch” configurations [25] of receiving PZT transducers are considered.

2. Experimental elastic characterization of the adopted unidirectional laminas

Both physical and elastic properties contribute to define the propagation velocities of an elastic wave in a given material [25], so, as a first step, the effective elastic moduli of the considered UD laminas were experimentally characterized. In particular, to completely define their linear elastic behaviour, unidirectional CFRP laminas require five independent elastic constant, so three different types of coupons (each composed of five specimens), representing the 0° UD, 90° UD and ±45° UD laminas, were designed according to ASTM-D 3039 [26] and ASTM-D 3518 [27] standards and subjected to experimental static tensile tests. The coupons allowed the definition of the in-plane tensile properties E_{11}, E_{22}, ν_{12} and ν_{21} of the single lamina constituting the laminate and, in a simplified way, of the in-plane shear modulus G_{12}. Regarding the fifth independent constant ν_{23}, the Christensen equation [28], relating ν_{23} to ν_{12} and ν_{21}, was applied.

An electro-mechanical tensile test machine MTS-Alliance RT/100 (maximum nominal load equal to 100 kN), an extensometer and two Wheatstone half bridges, dedicated to the longitudinal and transversal strains and compensated for temperature effects by “dummy” gages, formed the experimental set-up. The strain gauges were of the Vishay CEA06250UT350 type. Figure 1 shows the stress-strain curves (derived from extensometer data), while Table 1 summarises the obtained experimental elastic moduli of the UD laminas. In the latter, μ stands for the mean value, σ for the standard deviation and CV is defined by the ASTM-D 3039 standard [26] as the coefficient of variation (σ/μ) of the tested sample. It is worth noticing the peculiar fragmentation of the experimental curves coming from the 0° coupons, due to the progressive onset of delaminating phenomena inside the specimens with the increasing load. This behaviour is not more deepened here, since the important part of the curves, for the present research, is the linear initial one that rules the elastic wave behaviour.

3. Dispersive behavior of ultrasonic Lamb waves in the target laminate

One important task, to be performed initially in designing any inspection technique based on Lamb Waves, is to choose the appropriate frequency regime in order to excite just the needed wave propagation modes.

Among several available approaches, the semi-analytical finite element (SAFE) one is an efficient way for numerically modelling the propagation of guided waves in composite laminates of arbitrary layup and cross-sectional geometry. Bartoli et al. [29] discuss all the details on this method and compares it to other available ones, like finite elements or pure analytical approaches. Focusing, here, on the SAFE method, two quadratic 1-D finite elements were used to model each of the 17 laminas constituting the quasi-isotropic laminate, according to the convergence studies by Bartoli et al. [29] for dispersive solutions. Four different directions of propagation were simulated: 0°, 30°, 60° and 90° with respect to the 0° fibre of the laminate. The numerically stable results are shown in Figures 2a to 2d in terms of phase velocity C_p against frequency. As highlighted in the polar phase velocity plot of Figure 2e, a reasonable level of quasi-isotropic behaviour is confirmed for the considered laminate.

An essential parameter for the SHM process could also be determined: the so-called [11] “cut-off frequency”, $f_{cut\text{-}off}$, which outlines the value of actuating frequency below which only the three fundamental Lamb wave propagation modes can exist: the symmetric one “S_0”, the anti-symmetric one “A_0” and the shear horizontal one “SH_0”. Figures 2a to 2d show no substantial differences for the $f_{cut\text{-}off}$ value (about 380 kHz), since the quasi-isotropic stacking sequence minimises the anisotropy level of the laminate. Hence, an excitation frequency below 380 kHz was always applied throughout this research work.

Knowing the numerical cut-off frequency allowed hypothesizing the PZT ceramic for the present Lamb wave-based SHM process and the design of the possible transducer. In particular, the geometrical features of the PZT were chosen so to optimise both the actuating ($f < f_{cut\text{-}off}$) and receiving (adequately far away from the resonant frequencies) stages. Based on these data, the PI PIC255 piezo-ceramic transducer, characterised by a diameter equal to 5 mm and a thickness equal to 1 mm, was finally adopted.

Due to the criticality, on the SHM process, of the $f_{cut\text{-}off}$ parameter and of the adopted transducers, the semi-analytical results were also experimentally validated, as described in the following Section.

3.1 Experimental validation of the semi-analytical finite element dispersion curves

In the following part of the present research, the interest is focused onto the fundamental anti-symmetric A_0 propagation mode due to its well-known characteristics [11]. For this reason, the semi-analytical A_0 group velocity C_g was compared to the experimental one in order to validate the SAFE numerical model. In particular, four PZTs (named PZT1, PZT2, PZT3 and PZT4) of the type chosen in Section 3 were bonded, onto a circular quasi-isotropic laminate (Fig. 3a), with an angular step of 30° with respect to the 0° fibre. The adopted transmission and reception set-ups are shown in Figures 3b and 3c, respectively.

The received experimental signals were post-processed through the Hilbert transform [11] in order to obtain the envelope of the wave packet and the C_g values according to:

$$C_g = \frac{\Delta x}{tof} \tag{1}$$

where Δx is the wave propagation path from the actuator to the given receiver and "tof" is the corresponding time of flight.

Given that the first numerical outputs from the eigenvalue-eigenvector SAFE solution are k (wavenumber) and ω (circular frequency) values, the semi-analytical group velocities were derived as:

$$C_g \stackrel{\text{def}}{=} \frac{\partial \omega}{\partial k} \cong \frac{\Delta \omega}{\Delta k} \tag{2}$$

As can be seen in Figures 4a to 4d, a good level of agreement can be found since the experimental values are included within a 15% band from the numerical ones. Deviations can be explained by the unavoidable experimental uncertainties such as, for example, misleading orientations of fibres with respect to the position of PZTs or presence of small manufacturing defects inside the laminate. Nevertheless, the good correspondence between numerical and experimental results allowed confirming the $f_{cut\text{-}off}$ value and the PIC255 [30] piezo-ceramic transducer as the suitable ones for the present SHM process.

4. An actuating strategy to obtain a single significant A_0 propagation mode

PZT-generated Lamb waves unavoidably and simultaneously contain multiple wave propagation modes, which superimpose and influence each other making the interpretation of the received signal a troublesome task. At present, most mode selection approaches are based on the rationale that a desired wave mode can be enhanced, while other undesired ones minimised, using the mutual interactions of an array of appropriately located and actuated PZTs. From this point of view, Su and Ye [11] report an easy way to activate selectively a desired Lamb mode by actuating a pair of PZT transducers symmetrically bonded on the upper and lower surfaces of a composite laminate. In particular, in-phase actuation is useful for obtaining the S_0 symmetric mode, while out-of-phase actuation for the A_0 anti-symmetric one.

The just-described approach was here experimentally verified adopting again the circular quasi-isotropic laminate already shown in Figure 3a, but instrumented with two actuating PZTs symmetrically bonded on either side. The actuating signal consisted in a 5 cycles sinusoidal tone burst having a peak-to-peak range equal to 30 V_{pp} and modulated by a Hanning window. This signal was received by PZT1, PZT2, PZT3 and PZT4 shown in Figure 3a. Before performing the analysis, all the received signals were post-processed as follows:

1. raw data were firstly elaborated using the discrete wavelet transform (DWT) for de-noising the signal. In particular, the 6th level Daubechies wavelet proved to be particularly effective;

2. then, the continuous wavelet transform (CWT) was applied in order to extract the wavelet coefficient corresponding to the maximum percentage of signal energy, i.e. to the nominal frequency of actuation. In this case, the Morlet wavelet proved to be quite effective;
3. finally, the signals were treated by the Hilbert transform, so to draw them in the time domain and in terms of their energy content.

Considering, as an example, the signal received along the 0° angular direction, Figure 5a shows the case of a single actuating PZT excited at 100 kHz. This is the reference case for the following discussion, since no mode selection approach is applied. As expected, both S_0 and A_0 are present and they show comparable amplitudes (S_0: 100 mV, A_0: 80 mV), which, on the other hand, are much lower than the actuating one (30 V_{pp}). Applying, then, in-phase excitation of the two actuating PZTs at 100 kHz (Fig. 5b), the enhancement of the S_0 mode is actually achieved (about 150 mV) with respect to the reference case, but along with the enhancement of the A_0 one (about 90 mV), suggesting a different experimental observation with respect to what reported by Su and Ye [11]. Moving to out-of-phase excitation of the two actuating PZTs at 100 kHz (Fig. 5c), the propagation modes still seem to be significant and comparable (both about 75 mV), denoting a slight loss of energy with respect to the reference case and again a discrepancy with the literature. Starting from these observations, other measurements were then performed varying the excitation frequency. It was found out that actuating a single PZT within the frequency range between 0 and 50 kHz, a single A_0 mode seems to be generated, whose magnitude can be further enhanced applying out-of-phase excitation (Fig. 5d). The S_0 mode is hidden into the electrical noise and tends to become significant approaching 50 kHz, but still remaining one order of magnitude lower than the A_0 one. A further increase of the frequency takes the situation back to the described cases where 100 kHz were applied. It is worth noticing that only the latter actuation strategy was able to provide a single A_0 propagation mode, while all the others always showed comparable A_0 and S_0 modes and, finally, no strategy could show a single S_0 one. Moreover, the magnitude of the single A_0 mode seems to be significantly higher (about 170 mV) than the reference case.

A generalized application of the discovered actuating strategy (Fig. 5c and 5d) is shown in Figure 6 for all the instrumented angular directions of the circular quasi-isotropic laminate (Fig. 3a). In particular, the ratio between the A_0 and S_0 amplitudes is reported vs. the actuating frequency. All propagation directions confirm that, at low frequency, the energy amount contained in the A_0 mode is significantly higher than the one in the S_0 one. Then, in the range from 75 to 100 kHz, the same ratios decrease abruptly and remain around the 0 dB axis until the cut-off frequency.

The observed discrepancies, with respect to the model and the results proposed by Su and Ye [11], can be explained considering the shapes of Lamb wave modes: in the case of a single PZT actuator, both symmetric and asymmetric modes can be excited because membrane action and bending are simultaneously present, whereas, from a theoretical point of view, a dual actuation provides pure membrane action when in-phase and pure bending when out-of-phase. Actually, focusing on A_0 mode, the strategy proves to be incisive as long as it generates the classical linear trend of strains, due to mechanical bending, through the thickness of the laminate. On the other hand, the higher the frequency, the higher the discrepancy between the induced strain and the expected one because mode shapes get more and more complex. Considering the adopted CFRP laminate, SAFE results already provide a severely distorted asymmetric mode shape at 100 kHz, as shown in Figure 7. The superposition of this effect and what described by Giurgiutiu [24] give the results reported in Figure 6. Moreover, experimental uncertainties, like slight misalignments of the dual pair of transducers or the adhesion quality, could contribute in a stochastic way to the aforementioned behaviour.

Anyway, this experimental evidence opens the promising possibility of implementing the SHM of a CFRP laminate via out-of-phase excitation of two PZT(s), bonded onto the surface, and a single A_0 propagation mode. In the following sections, the set up approach is applied to study, according to DOE/ANOVA statistical approaches, its main influencing factors and performance when artificial and natural delaminations are present in the laminate.

5. Application of the set up actuating strategy to the detection of artificial delaminations

The performance analysis of the set up SHM approach is here carried out adopting a 2^k full-factorial statistical plan ([24], where k is the number of considered key factors and 2 the number of considered levels for each factor) in order to screen and identify the key influencing factors. Screening can also suggest the optimal settings, for such investigated factors, to be subsequently achieved by dedicated optimization plans. The interesting issue, in the application of DOE/ANOVA methodologies, is that the levels of the considered factors are simultaneously varied, allowing the study of mutual interactions. This is significantly more robust with respect to the traditional and very common “one-parameter-at-a-time” strategy [24], which is rarely the most efficient, because does not allow exploring all the possible combinations of factors in a feasible and affordable way.

The adopted statistical tool is, then, the “Analysis of Variance” [24]. In particular, the total Sum of Squares SS_{tot}, i.e. a measure of deviation from the mean value, is partitioned into different contributions. These are related to “residuals” SS_e, i.e. errors whose distribution is assumed to be normal with null mean value, and to the factors SS_f. In particular, the following matrix notation, in order to describe the relationship between the vector response variable $\{Y\}$ and the modelled vector factors {X} (plus the error $\{\varepsilon\}$), can be adopted:

$$\{Y\} = [\beta] \cdot \{X\} + \{\varepsilon\} \tag{3}$$

where $[\beta]$ is a matrix containing the coefficients of linear regression. The total Sum of Squares can then be easily written as:

$$SS_{tot} = SS_e + SS_f = \sum_{i=1}^{n} {y_i}^2 - \frac{(\sum_{i=1}^{n} y_i)^2}{n} \tag{4}$$

where y_i is the i-th element of [Y] and n the total number of observations, whereas:

$$SS_f = \left[\hat{\beta}\right]^T \{X\}^T \{Y\} - \frac{(\sum_{i=1}^{n} y_i)^2}{n} \tag{5}$$

where the hat sign (^) stands for the estimated coefficients of regression from the least squares estimation and, consequently:

$$SS_e = SS_{tot} - SS_f \tag{6}$$

Briefly, the SS_e is the variation attributed to the error, whereas SS_f is the one attributed to the relationships between the response and the investigated factors. By comparing SS_{tot} and SS_f, the portion of the total variation due to the key factors is found and quantified by R^2, the "coefficient of determination". Converting the Sum of Squares into mean squares (MS) by their degrees of freedom and dividing the MS_f (for the factors) by the MS_e (for the error) leads to a statistical F-test, where, setting a suitable p-value, the significance of the factors and their interactions can be inferred. All the described parameters are usually reported and provided in resulting ANOVA tables. Moreover, "main effects" and "interaction" plots are also often provided to show differences among level means. These plots give a first synthetic view of the results, but conclusions on statically significant patterns must be drawn on the appropriate F-tests. More details on factorial plans and ANOVA analyses can be found in [24].

Starting with the first step of analysis, the one properly named DOE, of the influencing factors, Figure 8a shows the 2^3 factorial plan designed for the considered case and requiring a total of eight different combinations of the chosen factors to be experimentally evaluated. To this aim, two different rectangular quasi-isotropic laminates were prepared, having dimensions equal to 800x450 mm^2 and both characterised by the same set of artificial defects, in order to have at least one replication of each measurement. Indeed, the concept of "replication", which is at the basis of the second step of analysis named ANOVA, means that the differences in responses obtained, from the two nominally identical artificially defected laminates, are due to the intrinsic uncertainties of the experiments and allow deriving information about the characteristic variance of the considered process.

The artificial defects were meant to represent delamination damages and were realized, during the manufacturing process, by suitably inserting circular Teflon patches between the plies. Nevertheless, the design factors, established amongst many others classified as fixed (influence of damage type, orientation, size and location, configuration of transducers, Lamb Wave modes, tone burst, …) and noise (influence of temperature, vibrations, electro-magnetic source, residual stresses …) factors, were: the actuating frequency, the dimension of artificial defects and their depth along the thickness of the laminate. In particular, the actuating frequency was set to 45 and 60 kHz, so across the aforementioned upper boundary of 50 kHz, in order to avoid the mutual scattering interference between boundary conditions and defects and to reach a compromise between sensitivity (the higher the frequency, the smaller the wavelength) and a minimum resolvable distance [31]. Artificial delaminations were characterised by diameters equal to 8 and 24 mm and were located between the first and second ply and the sixteenth and seventeenth ply, i.e. at depths of 0.125 mm and 2 mm from the upper surface, respectively (Fig 8b). It is important to add that all the described factor levels were sufficiently far-between to prevent the experimental standard deviation could hide the significance of the factors under investigation. Table 2 provides the codification of the design factors adopted for the ANOVA described in the following Sections.

Ten PZT transducers, then, instrumented each laminate: two for the actuation (one on either side), four dedicated to Pulse-Echo (PE) measurements and the remaining four to Pitch-Catch (PC) ones (Fig. 8b). In order to check the real final dimension of the artificial defects and their relative position with respect to the sensors, x-ray radiographs of all the defects were performed applying 28 kV and 5 mA for 30 s. Figure 8c shows an example radiography of one of the artificial defects having diameter equal to 24 mm.

Finally, just out-of-phase excitation of the actuating PZTs was considered and both the excitation signal and the post-processing methodology of the received signals corresponded to those already described in Section 4.

5.1 Statistical analysis of Pulse-Echo measurements

Considering pulse-echo (PE) measurements, the response to artificial damages was recorded in terms of the reflection coefficient R, which is here defined as the ratio between the largest amplitude of the first damage-reflected A_0 wave component captured by the sensor (subscript “r”) and that of the incident wave (subscript “i”):

$$R = \frac{CWT_r}{CWT_i} \tag{7}$$

where CWT is the coefficient of the continuous wavelet transform of the given signal along its central frequency scale axis.

The statistical analysis was then performed in order to derive the influence of the design factors, described in Section 5, on the reflection coefficient R. In particular, the “main effects” and the “interaction” plots (Fig. 9a and 9b, respectively) outline, as relevant factors, the diameter and the “frequency-diameter” interaction and, in a weaker form, the diameter and the “diameter-depth” interaction. These conclusions could be drawn observing that different levels of a factor affect the response in a different way and, consequently, the model line is not horizontal: the steeper the slope of the line, the greater the magnitude of the considered main effect or interaction. Contrarily, the basics of an ‘’interaction” plot is the presence of parallelism or not within the plotted lines: parallel ones indicate no interaction, whereas the greater the difference in slope between them, the higher the degree of interaction Anyway, these results are somehow subjective and doesn’t reveal if the interaction is statistically significant. Hence, a more statistically rigorous ANOVA is needed to highlight any significant influence on the variance of the process.

Assuming a fixed and suitable “level of significance” (“α-value”, here set to 10%), the ANOVA results (Tab. 3) for the complete model, i.e. all factors and their interaction are considered, point out that the “frequency-diameter” interaction is indeed the key factor influencing the PE process applied to artificial delaminations, since its p-value is comparable to the chosen α one. The frequency, which seemed to be also significant from the “main effects” plot as a stand-alone factor, is instead not so strong to justify such conclusion, i.e. its p-value is significantly higher than the chosen α one. The depth, the diameter and all the other interactions are not highlighted by the ANOVA. The verification of the statistical hypotheses, shown in Figure 9c, supports these conclusions in terms of the test of normality, homogeneity of variance, absence of structure of the residuals and their independence from run-order.

Starting from the results of the complete statistical model a “reduced” one was built considering just the highlighted interaction and, for completeness, its involved factors. The resulting model, summarised in Table 3, fits the experimental evidence better than the complete one, since the R^2_{adj} parameter gets higher, while the R^2 parameter always increases with the number of predictors in the model.

Considering again Table 3 and Figure 9b, the PE performance, with respect to the larger defects, seems to be rather independent from the actuation frequency. On the other hand, the detection of the smallest ones can be enhanced working at higher frequency. These phenomena can be explained by the smallest wavelength achievable working at higher frequencies, which guarantees a better defect-wave interaction, but, as the damage extension reaches an adequate ratio between the diameter of the defect and the wavelength, it seems to give back a steady response. It is worth emphasising that the depth of the defect inside the laminate, with respect to the transducers position, does not seem to influence the PE SHM configuration.

The final response, of the PE technique applied to an artificial delamination by means of its reflection factor R, can then be expressed and quantified, by the coefficients reported in Table 3, as the following predictive empirical model:

$$R = 0.04344f + 0.01036D - 0.05622(f * D) \tag{8}$$

where f is the central frequency of the pulse, D the diameter of the artificial defect. Eq. (8) is the linear regression output of the ANOVA applied to the reduced model of the 2^3 factorial plan, taking into account the 37.38% of the overall variance as showed by the R^2coefficient of Table 3. Eq. (8) highlights that the dependence of damage detection sensitivity is not on the actuation frequency and size of damage (which is actually intuitive), but on the actuation frequency, size of damage and the multiplication between the actuation frequency and the size of damage (which is less intuitive). Neglecting the last contribution (f*D), as usually done adopting "one-parameter-at-a-time" strategies, would make any predictive models someway incomplete.

5.2 Statistical analysis of Pitch-Catch measurements

Regarding the Pitch-Catch (PC) configuration, the response to artificial damages was instead recorded in terms of the transmission coefficient T, which is here defined as the ratio between the largest amplitude of the damage-transmitted A_0 wave component captured by the sensor (subscript "t") and that of the incident wave (subscript "i"):

$$T = \frac{CWT_t}{CWT_i} \tag{9}$$

where CWT is again the coefficient of the continuous wavelet transform of the given signal along its central frequency scale axis.

In this case, the “main effects” and “interaction” plots (Fig. 10a and 10b, respectively) outline a strong dependency on the diameter of the defect and a weak “diameter-depth” interaction. Moreover, Figure 10c shows the effectiveness of the 2^3 factorial plan hypothesis about the residuals: normality, homogeneity of variance, absence of structure and independence from run-order.

The ANOVA analysis of the complete model of the sampled data (Tab. 4) points out, assuming again α=10%, the diameter as the potential key factor influencing the Pitch-Catch SHM based process. Consequently, a reduced model was built, only considering the diameter factor: as expected, Table 4 fits the experimental evidence better, since the R^2_{adj} parameter gets higher.

In summary, the PC response to an artificial delamination defect is influenced by its extension only, regardless the diagnostic wave excitation frequency and the position of the defect along the thickness of a CFRP laminate. Nevertheless, abrupt changes in the amplitude response signal to diagnostic wave occurs when the A_0 mode is transmitted through them.

The final response, of the PC technique applied to an artificial delamination by means of its transmission factor T, can be expressed and quantified, by the coefficients reported in Table 4, as the following predictive empirical model:

$$T = 0{,}3344 - 0{,}0731D \tag{10}$$

where D is the defect diameter. As aforementioned reported, Eq. (10) comes out from the reduced model and explains, by the significant predictor D, the 37.78% of response variability (Tab. 4). This is a useful result because it demonstrates, on a rigorous and robust way and contrarily to what found for PE measurements, the possibility to apply more simple predictive models for PC ones.

6. Application of the set up actuating strategy to the detection of natural delaminations

Artificial defects are usually adopted to calibrate NDT or SHM instruments and to check the performance of inspecting procedures because easier to realize, size, verify and inspect, but their capability to represent real defects is often questioned in the literature. For this reason, the performance of the set up actuating strategy was also evaluated considering delamination-like damages introduced in CFRP laminates by drop weight impact tests. In particular, low-velocity impacts were performed, since they can cause a significant amount of internal delamination against very small or even invisible surface indentation. This type of damage is often referred to [3] as "Barely Visible Impact Damage" (BVID) and it can cause a significant degradation of the structural properties and strength. Boeing [3] defines BVID as: "small damages which cannot be found during heavy-maintenance general visual inspections using typical lighting conditions from a distance of five feet".

Impact tests were performed, according to ASTM D7136 [32], using a 25.4 mm diameter hemispherical tip weight (Fig. 11a), whose mass was about 1.2 kg, guided by an impact device consisting of a cylindrical tube mechanism, as shown in Figure 11b. The impact device was equipped (Fig. 11c) with a Mel M7L laser triangulation sensor in order to acquire the real impact velocity, and the consequent real impact energy, by the ratio between the length and the time of flight of the sampled weight shape during flight (Fig. 11d). After impact tests, the target CFRP laminate (Fig. 12a) presented four different impact locations: Table 5 shows the real obtained impact energies for each of them. Figure 12b shows a detail of the region impacted by the highest energy (20 J): none of the common externally visible damage modes [32], such as dent/depression or splits/cracks, is visible, hence the barely visible condition was achieved. On the other hand, the correct onset of a real damage was checked by an ultrasonic phased array equipment (Harfang X32 flaw detector and a 32 active crystals probe working at 10 MHz) adopting a through-thickness L-Scan visualization. Figure 12c shows the example of the same region shown in Figure 12b: a significant BVID damage was actually achieved.

The impacted laminate was instrumented by a central pair of PZT actuators, out-of-phase energised at 45 and 60 kHz, and an array of PZT sensors so to perform both the PC and the PE SHM techniques and the sampled data were then digitally processed, by the same methodology already described in Section 5 about artificial defects. Considering, in this case, the implementation of a 2^2 full factorial statistical plan, the design factors were limited to impact energy and actuating frequency, whose DOE high-low coded values were 5 and 20 J for the former and 45 and 60 kHz for the latter. In particular, the impact energy was here assumed to be directly and proportionally related to the extension of damage. On the other hand, the morphology of a natural impact damage is very complex because it is the combination of three types of damage [4]: matrix cracks, fibre fractures and delaminations, each of which contribute to the global response. For this reason, the definition of a depth of the delamination is a nonsense and this design factor was not considered. Finally, a rigorous ANOVA analysis could not be performed, since the number of replications per factor level was limited to one (the impacted CFRP laminate was just one), so there was not enough experimental data to estimate the variance of the process. Anyway, preliminary conclusions could be drawn in terms of “main effects” and “interaction” plots (Fig. 13). In the “main effects” plot, inclined lines mean that different levels of the factors affect the mean response and the steeper the slope, the greater the effect. The “interaction” plot, instead, allows visualizing possible interactions based on different line slopes.

On the subject, the response of the implemented SHM process showed a good level of similarity with respect to the case of artificial defects. In particular, the PE method underlined the same kind of “frequency-energy (diameter)” interaction, where the response is maximised driving the PZT at higher frequencies considering small defects, i.e. obtained by low energy impacts, whereas it is almost steady when interacting with large defects. A discrepancy consisted, instead, of the apparent significance, i.e. not based on the estimation of the variance of the process, of the energy and the frequency as standalone factors. Their influence onto the reflection factor R can be attributed to the very complex morphology of a natural BVID damage with respect to artificial delaminations simulated through a Teflon patch. This opens the promising possibility to extract, from the response signal, additional information about the nature of damage.

On the other hand, the PC method was mainly influenced by the extension of the defect, i.e. the impact energy: the higher the extension, the lower the transmission coefficient T. Hence, in that case, the complex damage mechanism does not seem to influence the final response of natural defects with respect to artificial ones.

It remains an insight into the physics of damage detection, by Lamb waves for the considered CFRP laminate, is now under study as a development of the research.

7. Concluding remarks

After having set up and experimentally characterised a Lamb wave mode tuning, combining a low frequency range and an out-of-phase actuation of a dual pair of actuators, for the most representative aeronautical quasi-isotropic CFRP laminate, a statistical approach, based on the “Design of Experiments” and the “Analysis of Variance” methodologies, has been applied to derive the key factors influencing the sensitivity response against artificial and natural delaminations. The results can be summarised:

- contrarily to commonly adopted mode tuning approaches, the proposed methodology is able to give back the single fundamental A_0 mode, suppressing other modes for frequencies up to 50 kHz;
- the actuating frequency range [0;50] kHz significantly simplifies the interpretation of diagnostic signal waves received by PZT sensors;
- significant elements of similarity between the responses to artificial and natural delaminations were found;
- Pitch-Catch responses are only reliant on the damage extension in the laminate;
- Pulse-Echo responses have good recollection of the complex damage mechanism in the host structure. This opens the promising possibility to extract, from the response signal, additional information about the nature of damage;
- knowing the key factors and how they play a role in the NDE, essential information are here supplied with the aim of design an optimized SHM PZT sensor network.

Acknowledgements

The authors would like to thank Mr. R. Galeazzi for the active help given to the present research.

References

[1] Harris CE, Starnes JH Jr, Shuart MJ. An Assessment of the State-of-the-Art in the Design and Manufacturing of Large Composite Structures for Aerospace Vehicles. Langley Research Center, Hampton, Virginia; 2001.

[2] Mallick PK. Fiber-Reinforced Composites. 3rd ed. CRC Press; 2007.

[3] Fawcett AJ, Oakes GD. Boeing Composite Airframe Damage Tolerance and Service Experience Boeing Commercial Airplanes 787 Program. 2012.

[4] Abrate S, Castanié B, Rajapakse YDS. Dynamic Failure of Composite and Sandwich Structures. 1st ed. New York: Springer; 2013.

[5] Soutis C. Carbon fibre reinforced plastics in aircraft structures. Mater Science and engineering A 2005;412:171-76.

[6] Bar-Cohen Y. Emerging NDE technologies and challenges at the beginning of the 3rd millennium—PartI. Mater Evaluation 2000;1:17–30.

[7] Bar-Cohen Y. Emerging NDE technologies and challenges at the beginning of the 3rd millennium – PartII. Materials Evaluation 2000;58:141–50.

[8] Boller C. Ways and options for aircraft structural health management. Smart Mater Struct 2001;10(3):432.

[9] Chang FK. Structural Health Monitoring: A Summary Report. Proceedings of the 2nd International Workshop on Structural Health Monitoring. Stanford, CA, September 8-10, 1999.

[10] Staszewski W, Boller C, Tomlinson G. Health monitoring of aerospace structures: smart sensor technologies and signal processing. 1st ed. New York: John Wiley & Sons Ltd; 2004.

[11] Su Z, Ye L. Identification of Damage Using Lamb Waves: From Fundamentals to Applications. 1st ed. Berlin: Springer;2009.

[12] R. Gutkin, Green CJ, Vangrattanachai S, Pinho ST, Robinson P, Curtis PT. On acoustic emission for failure investigation in CFRP: Pattern recognition and peak frequency analyses. Mechanical Systems and Signal Processing 2011;25:1393-407

[13] Lamb H. On Waves in an Elastic Plate. Proc R Soc Lond A 1917;93.

[14] Lemistre M, Balageas D. Structural health monitoring system based on diffracted Lamb wave analysis by multiresolution processing. Smart Mater Struct 2001;10:504-11.

[15] Su Z, Ye L. Lamb wave-based identification technique for delamination in composite laminates using artificial neural algorithm. Compos Struct 2004;66:627-37.

[16] Kessler SS, Spearing SM, Soutis C. Damage detection in composite materials using Lamb wave methods. Smart Mater Struct 2002; 11:269-78.

[17] Biemans C, Staszewski WJ, Boller C, Tomlinson GR, Crack detection in metallic structures using piezoceramic sensors. Key Eng Mater 1999; 167/168 112-21.

[18] Valle C, Littles JWJr. Flaw localization using the reassigned spectrogram on laser-generated and detected Lamb modes. Ultrasonics 2002; 39 535-42.

[19] Silva MZ, Gouyon R, Lepoutre F. Hidden corrosion detection in aircraft aluminum structures using laser ultrasonics and wavelet transform signal analysis. Ultrasonics 2003;41:301-5.

[20] Wong BS, Williams R. Non-destructive testing methodologies of advanced composite materials New Challenges in Aircraft Maintenance and Engineering Conference. Singapore; 1990.

[21] Kim SB, Hoon S. Instantaneous reference-free crack detection based on polarization characteristics of piezoelectric materials. Smart Materials and Structures 16;2007:2375.

[22] Giurgiutiu V. Tuned Lamb wave excitation and detection with piezoelectric wafer active sensors for structural health monitoring. Journal of intelligent material systems and structures 16;2005:291-305.

[23] Toso N, Alastair J. LIBCOS-Significance of Load upon Impact Behavior of Composite Structure. Research Project EASA 2009/3;2011.

[24] Montgomery DC. Design and Analysis of Experiment. 8th ed. New York: John Wiley & Sons Ltd; 2012.

[25] Krautkramer J, Krautkramer H, Ultrasonic Testing of Materials. 4th ed. Berlin:Springer-Verlag; 1990.

[26] ASTM D3039/D3039M-08. Standard Test Method for Tensile Properties of Polymer Matrix Composite Materials. ASTM International 2008.

[27] ASTM D3518/D3518M-94. Standard Test Method for In-Plane Shear Response of Polymer Matrix Composite Materials by Tensile Test of a ±45° Laminate. ASTM International 2007.

[28] Christensen RM. The Numbers of Elastic Properties and Failure Parameters for Fiber Composites. J Eng Mater Technol 1998;120:110-13.

[29] Bartoli I, Marzani A, Lanza di Scalea F, Viola E. Modeling wave propagation in dumped wave guides of arbitrary cross-section. J of Sound Vib 2006; 285:685-707.

[30] PiCeramic. Piezo Material Data. www.piceramic.com. 2012.

[31] Wilcox P, Lowe M, Cawley P. The effect of dipersion on long-range inspection using ultrasonic guided waves. NDT&International 2001;34:1-9.

[32] ASTM D7136/D7136M-12. Standard Test Method for Measuring the Damage Resistance of a Fiber-Reinforced Polymer Matrix Composite to a Drop-Weight Impact Event. ASTM International 2007.

List of Tables

	E_{11} [GPa]	**ν_{12}**	**E_{22} [GPa]**	**ν_{21}**	**ν_{23}**	**G_{12} [GPa]**	**ρ [Kg/m^3]**
μ	159.4	0.32	8.1	0.018	0.46	4.7	1550
σ	2.5	0.019	0.43	0.001	/	0.34	/
CV [%]	1.6	5.8	5.3	7.5	/	7.3	/

Tab. 1

Factor	Frequency f [kHz]		Depth d [mm]		Diameter D [mm]	
	Physical Value	***ANOVA Code***	***Physical Value***	***ANOVA Code***	***Physical Value***	***ANOVA Code***
	45	-1	0.125	-1	8	-1
	60	+1	2	+1	24	+1

Tab. 2

				Complete Model				
	Constant	f	D	d	f*D	f*d	D*d	f*D*d
p-Value	0,001	0,189	0,741	0,885	0,100	0,625	0,314	0,964
R-sq				46.92%				
R-sq(adj)				0,48%				
				Reduced Model				
	Constant	f	D	-	f*D	-	-	-
p-Value	0,000	0,131	0,706	-	0,058	-	-	-
R-sq				37,38%				
R-sq(adj)				21,72%				

Tab. 3

Complete Model								
	Constant	f	D	d	f*D	f*d	D*d	f*D*d
p-Value	0,000	0,0742	0,040	0,908	0,925	0,671	0,248	0,854
R-sq				49.83%				
R-sq(adj)				5.92%				
Reduced Model								
	Constant	-	D	-	-	-	-	-
p-Value	0,000	-	0,011	-	-	-	-	-
R-sq				37,78%				
R-sq(adj)				33,33%				

Tab. 4

Nominal impact energy [J]	**Drop height [m]**	**Measured impact velocity [m/s]**	**Real impact energy [J]**
5	0.4	2.03	2.8
10	0.8	3.7	8.1
15	1.2	4.8	13.8
20	1.7	5.9	20.8

Tab. 5

List of Figures

Figure 11 – Detail of the experimental set-up used for the drop weight impact tests: a) adopted weight; b) measurement chain and impact device; c) laser triangulation for real impact velocity determination; d) example of laser acquisition of the falling weight.

Figure 12 – Target CFRP laminate subjected to drop weight impact tests. The red ellipses identify the zones impacted at different energies.

Figure 13 – Statistical analysis of the effect of the design factors on the detection of natural delaminations: a) "main effects" plot for the reflection coefficient in PE inspection; b) "interaction" plot for the reflection coefficient in PE inspection; c) "main effects" plot for the transmission coefficient in PC inspection; d) "interaction" plot for the transmission coefficient in PC inspection.

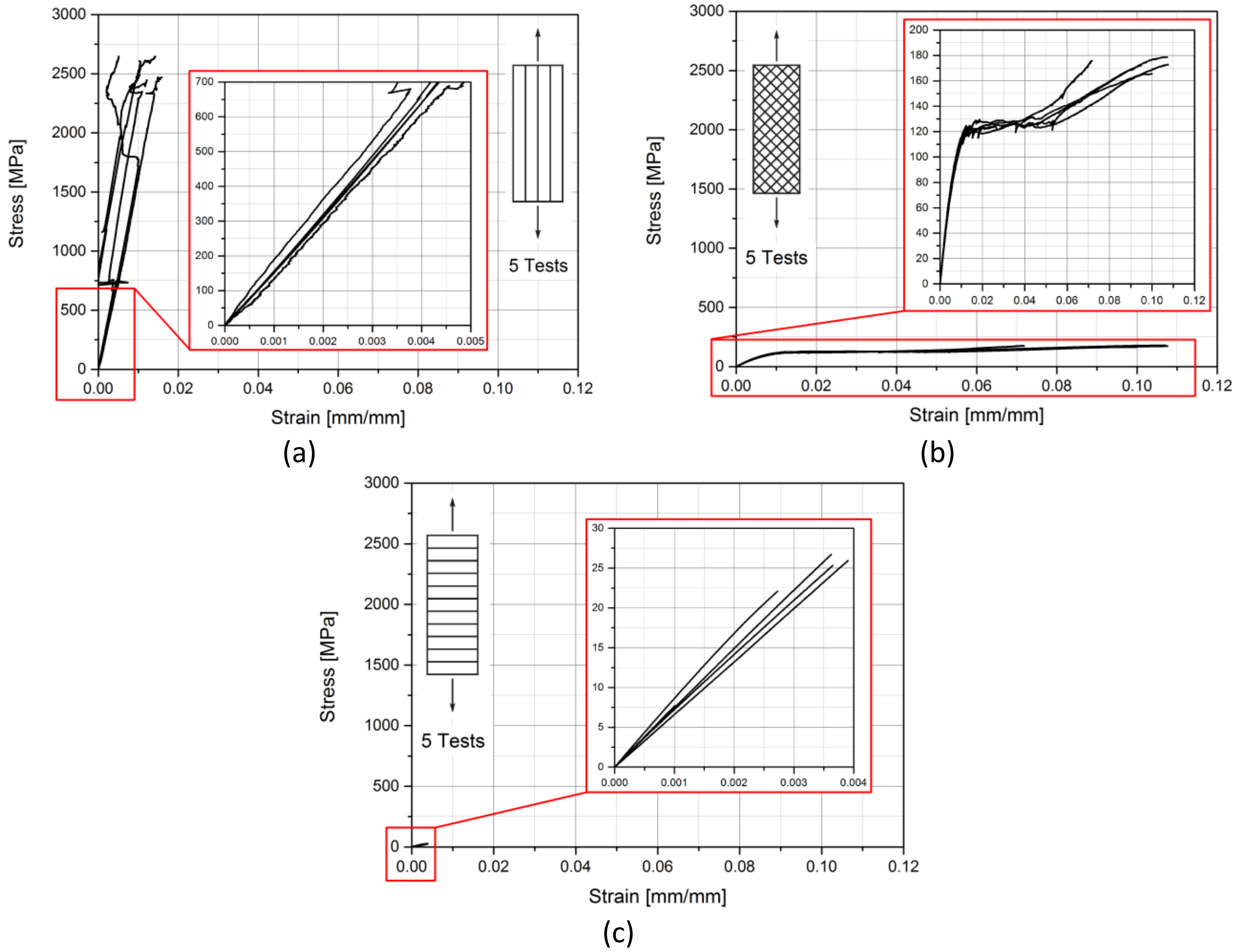

Fig. 1

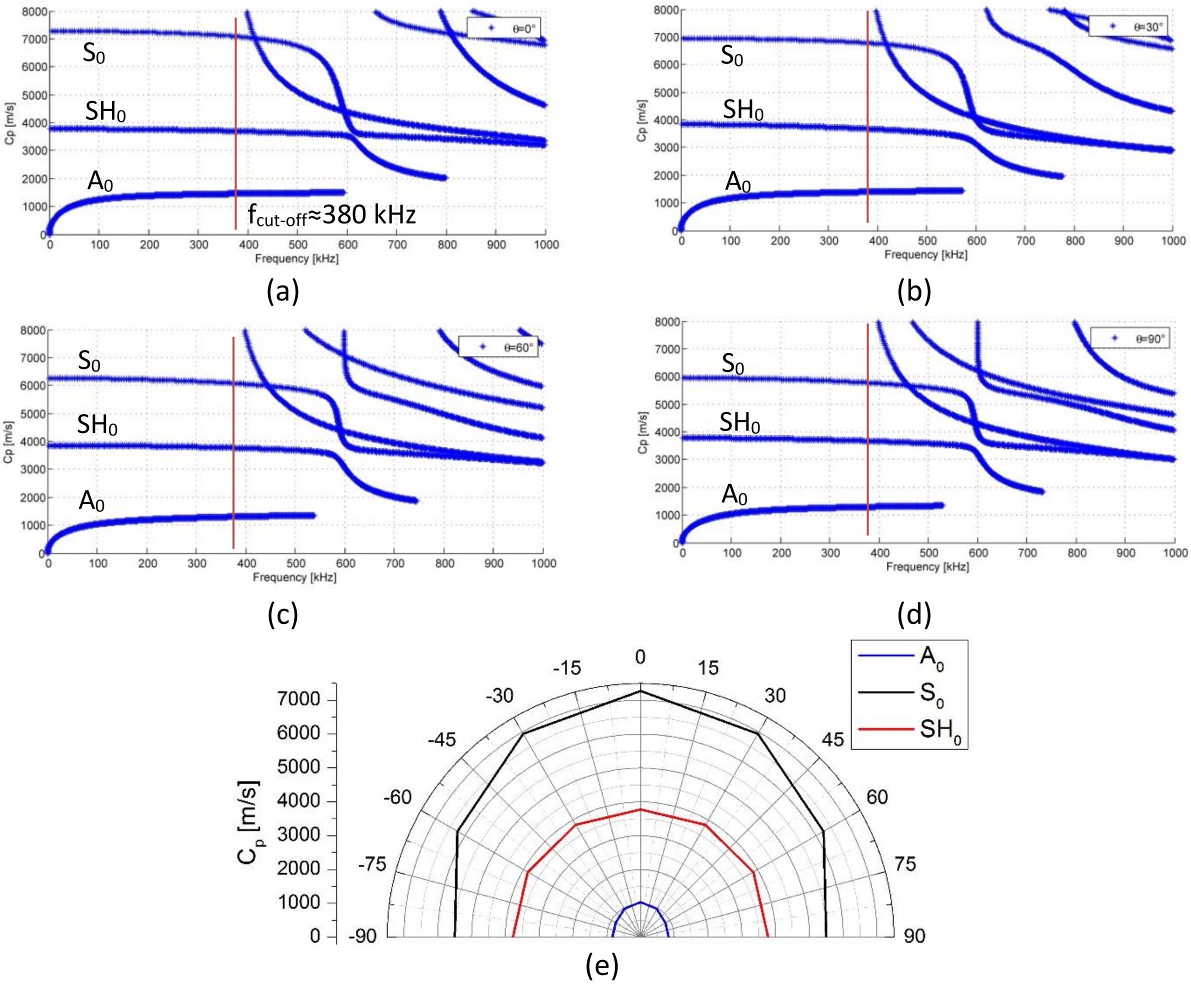
θ=0°
S0
SH0
A0
f_cut-off≈380 kHz
Cp [m/s]
Frequency [kHz]
(a)
θ=30°
(b)
θ=60°
(c)
θ=90°
(d)
A0
S0
SH0
Cp [m/s]
(e)

Fig. 2

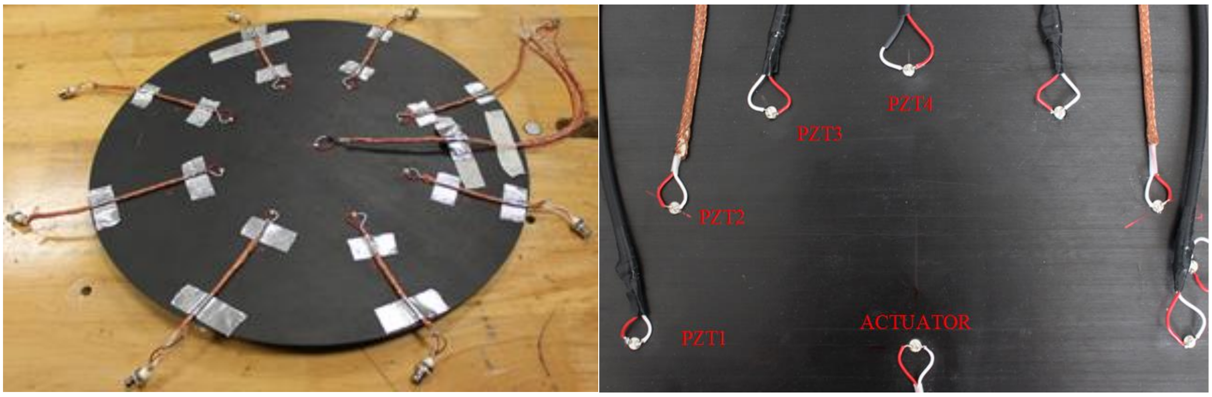
PZT4
PZT3
PZT2
PZT1
ACTUATOR

(a)

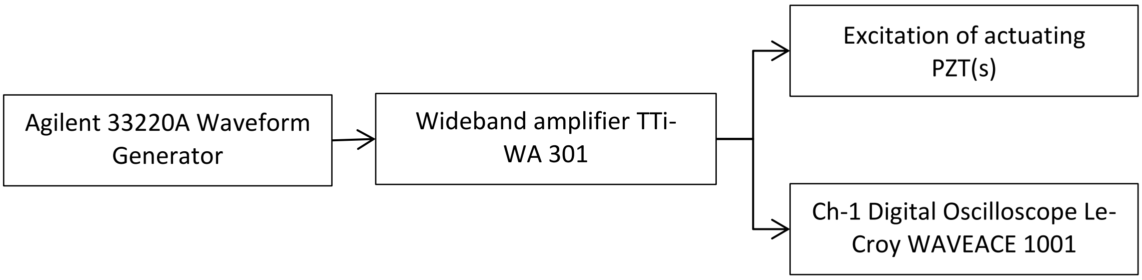
Agilent 33220A Waveform Generator
Wideband amplifier TTi-WA 301
Excitation of actuating PZT(s)
Ch-1 Digital Oscilloscope Le-Croy WAVEACE 1001

(b)

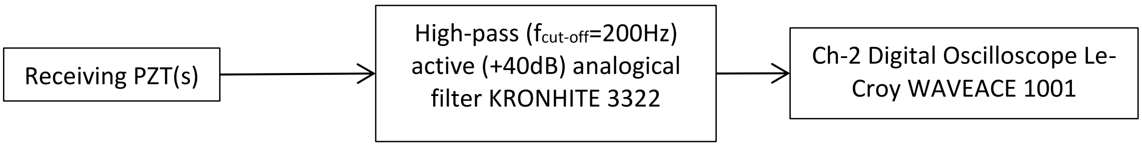
Receiving PZT(s)
High-pass ($f_{cut-off}$=200Hz) active (+40dB) analogical filter KRONHITE 3322
Ch-2 Digital Oscilloscope Le-Croy WAVEACE 1001

(c)

Fig. 3

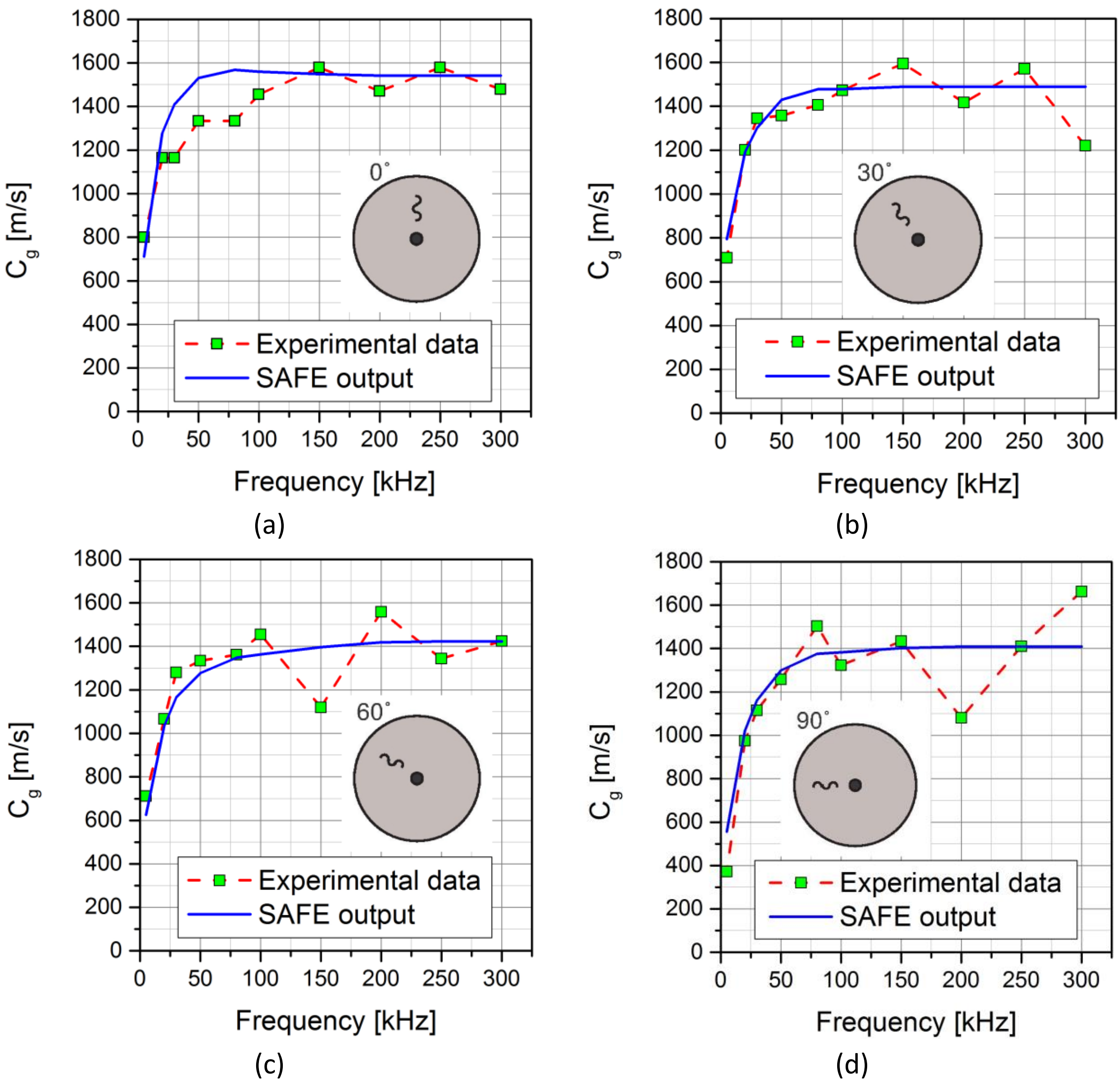

(a)
0˚
(b)
30˚
(c)
60˚
(d)
90˚
C_g [m/s]
Frequency [kHz]
Experimental data
SAFE output

Fig. 4

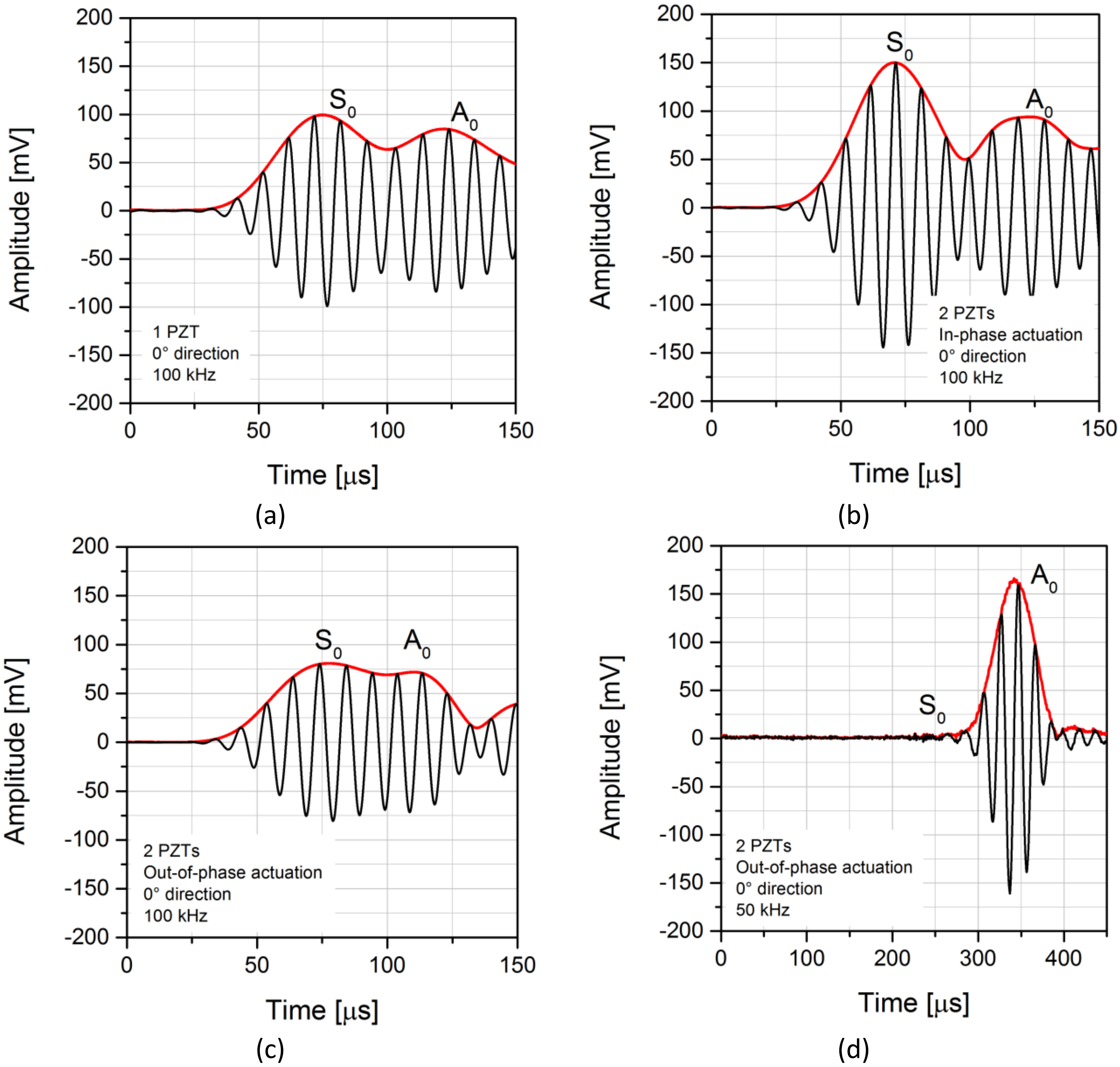

(a)
Amplitude [mV]
Time [µs]
S0
A0
1 PZT
0° direction
100 kHz
(b)
Amplitude [mV]
Time [µs]
S0
A0
2 PZTs
In-phase actuation
0° direction
100 kHz
(c)
Amplitude [mV]
Time [µs]
S0
A0
2 PZTs
Out-of-phase actuation
0° direction
100 kHz
(d)
Amplitude [mV]
Time [µs]
S0
A0
2 PZTs
Out-of-phase actuation
0° direction
50 kHz

Fig. 5

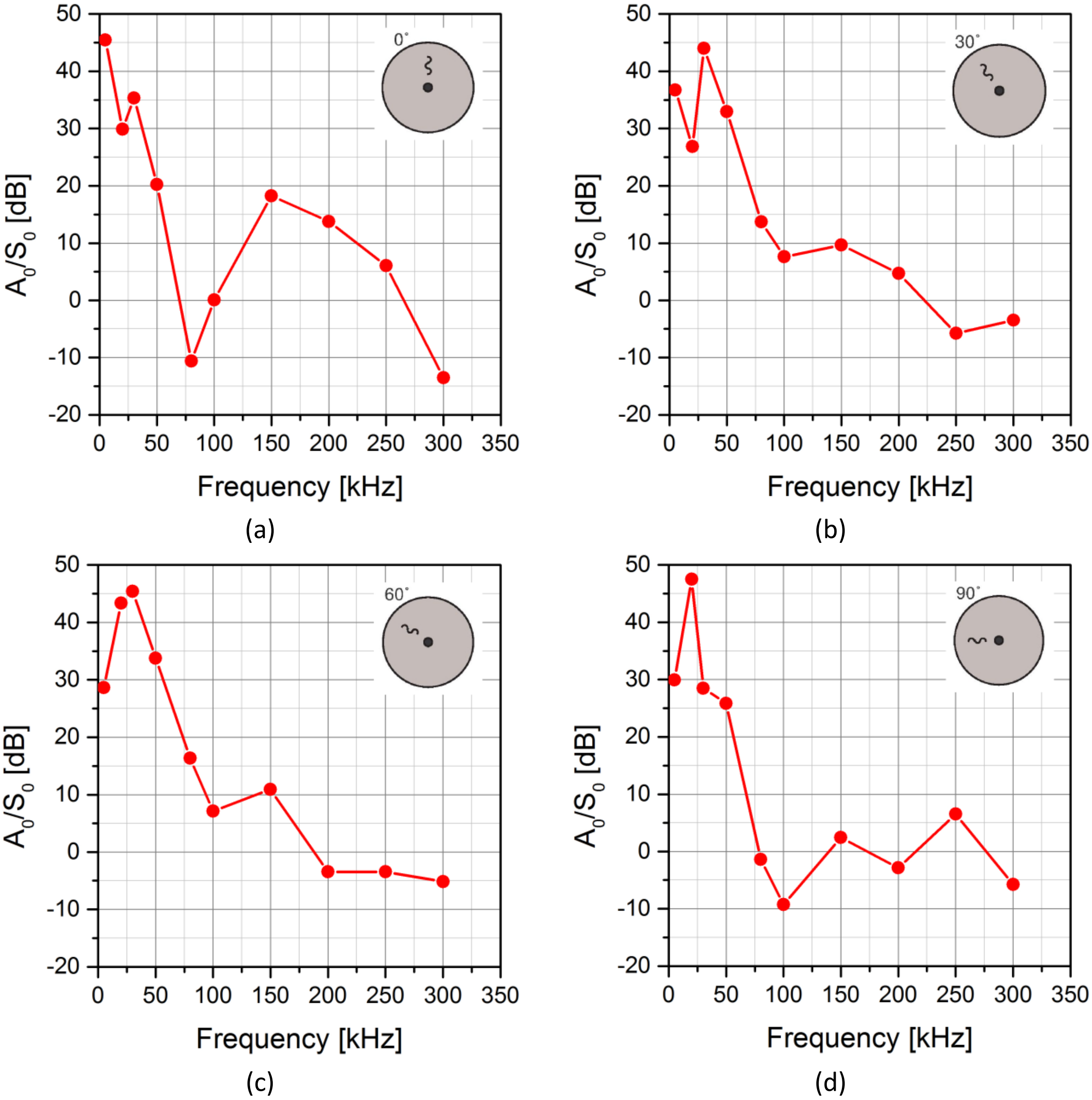
0°
30°
60°
90°
A0/S0 [dB]
Frequency [kHz]
50
40
30
20
10
0
-10
-20
0
50
100
150
200
250
300
350
(a)
(b)
(c)
(d)

Fig. 6

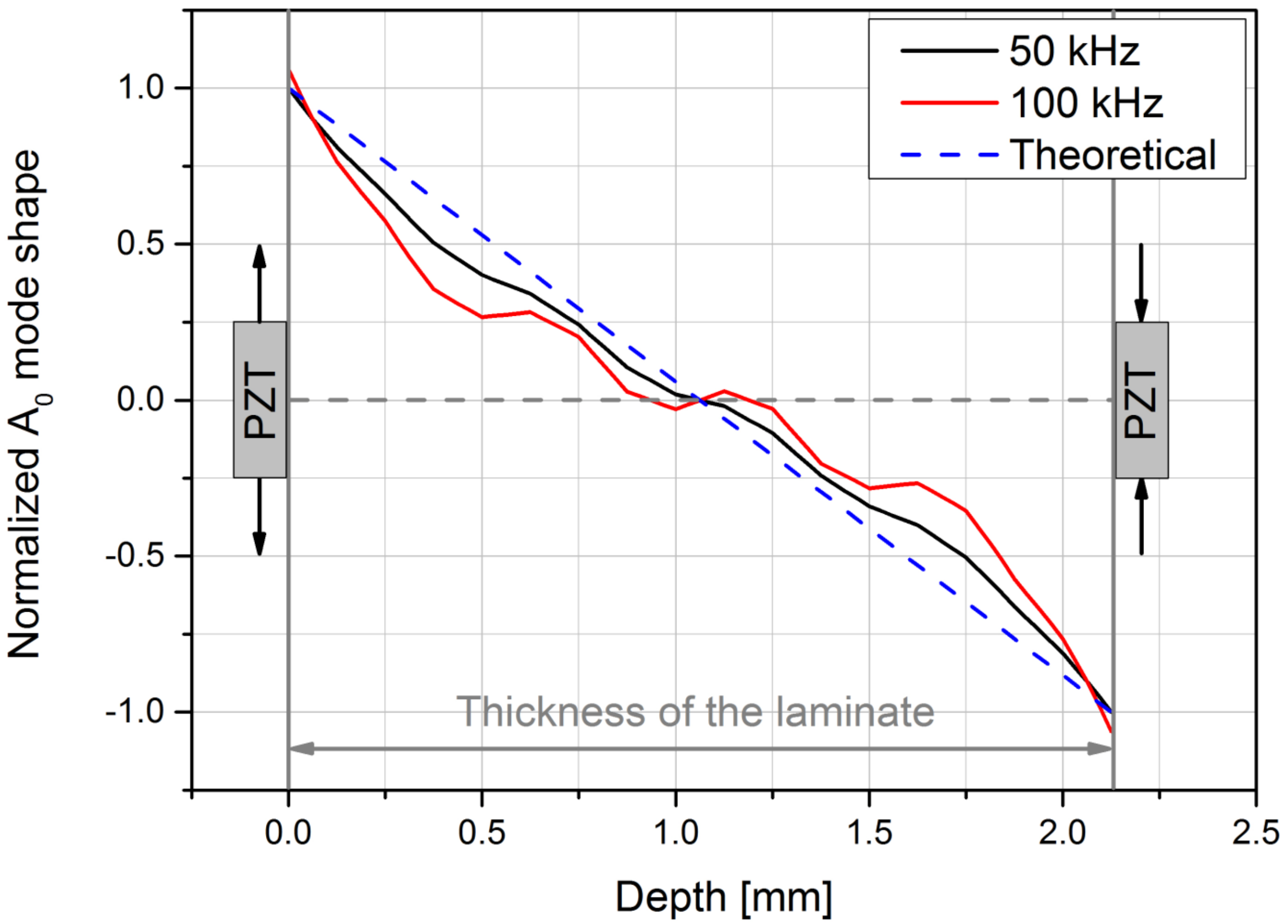

50 kHz
100 kHz
Theoretical
PZT
PZT
Thickness of the laminate
Normalized A_0 mode shape
Depth [mm]
1.0
0.5
0.0
-0.5
-1.0
0.0
0.5
1.0
1.5
2.0
2.5

Fig. 7

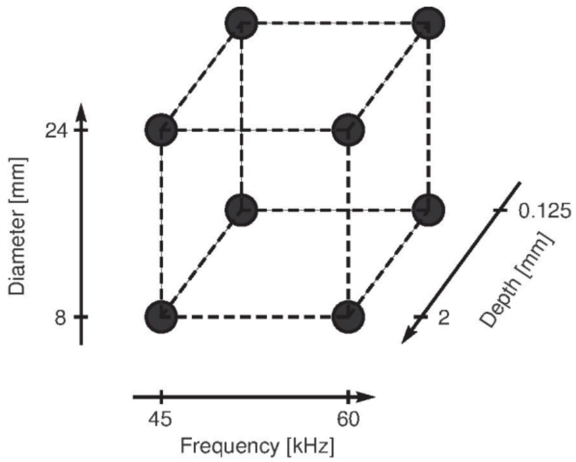
24
8
Diameter [mm]
0.125
2
Depth [mm]
45
60
Frequency [kHz]

(a)

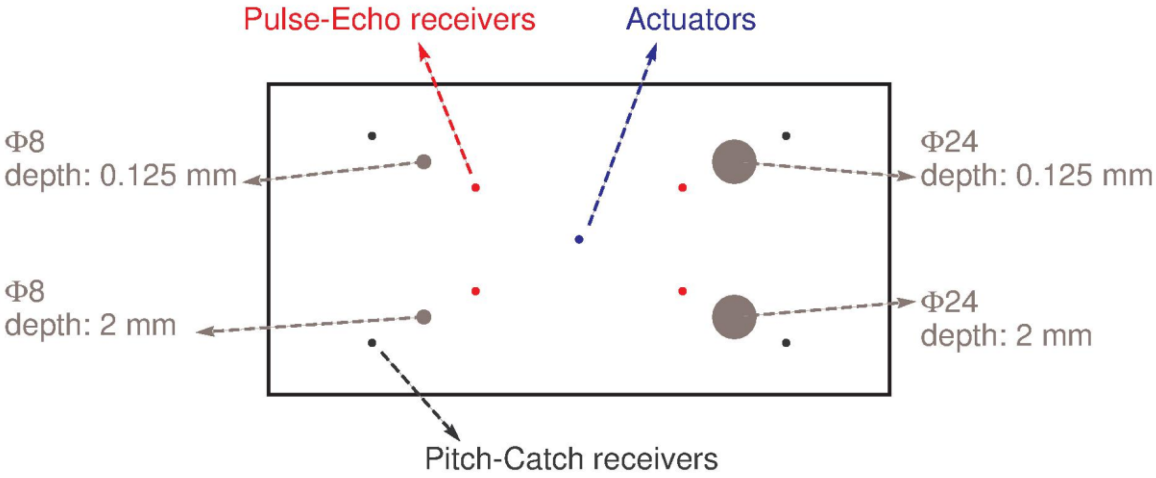
Pulse-Echo receivers
Actuators
Φ8
depth: 0.125 mm
Φ8
depth: 2 mm
Φ24
depth: 0.125 mm
Φ24
depth: 2 mm
Pitch-Catch receivers

(b)


26-6 -2013
PR6

(c)

Fig. 8

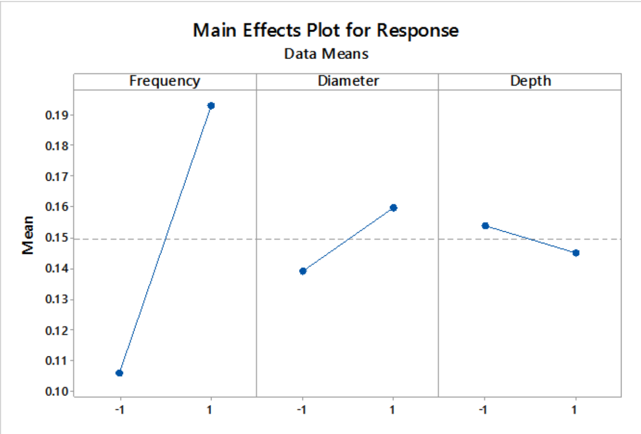
Main Effects Plot for Response
Data Means
Frequency
Diameter
Depth
Mean
0.19
0.18
0.17
0.16
0.15
0.14
0.13
0.12
0.11
0.10
-1
1
-1
1
-1
1

(a)

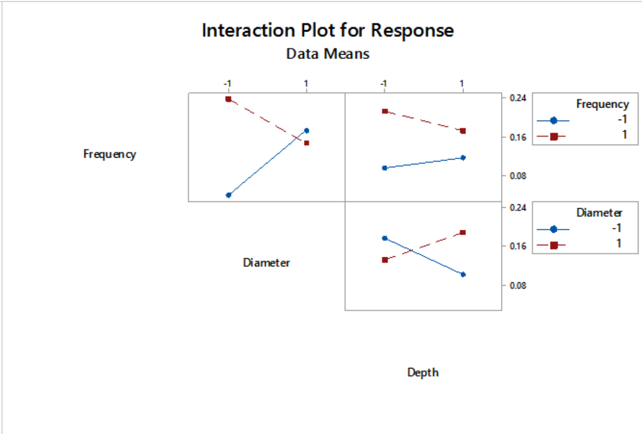
Interaction Plot for Response
Data Means
-1
1
-1
1
Frequency
Diameter
Depth
0.24
0.16
0.08
0.24
0.16
0.08
Frequency
-1
1
Diameter
-1
1

(b)

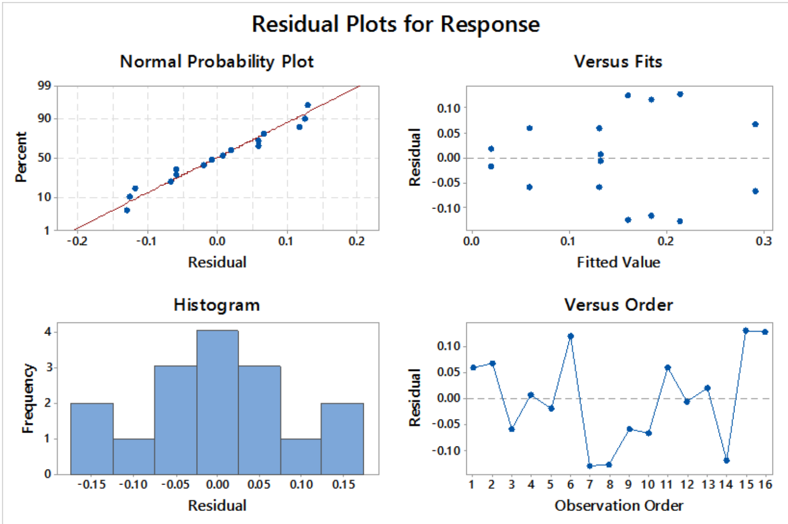
Residual Plots for Response
Normal Probability Plot
Percent
99
90
50
10
1
-0.2
-0.1
0.0
0.1
0.2
Residual
Versus Fits
Residual
0.10
0.05
0.00
-0.05
-0.10
0.0
0.1
0.2
0.3
Fitted Value
Histogram
Frequency
4
3
2
1
0
-0.15
-0.10
-0.05
0.00
0.05
0.10
0.15
Residual
Versus Order
Residual
0.10
0.05
0.00
-0.05
-0.10
1 2 3 4 5 6 7 8 9 10 11 12 13 14 15 16
Observation Order

(c)

Fig. 9

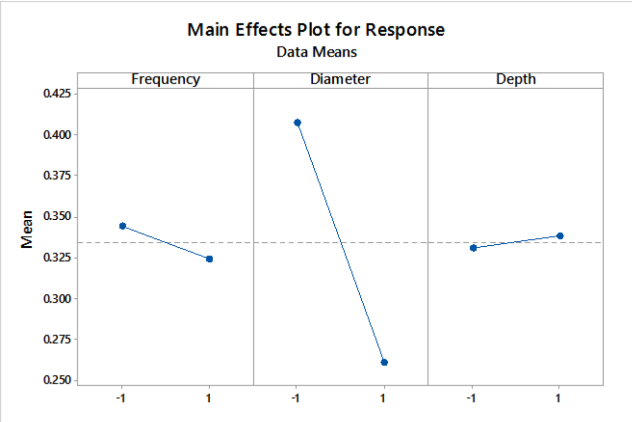

Main Effects Plot for Response
Data Means
Frequency
Diameter
Depth
Mean
0.425
0.400
0.375
0.350
0.325
0.300
0.275
0.250
-1
1

(a)

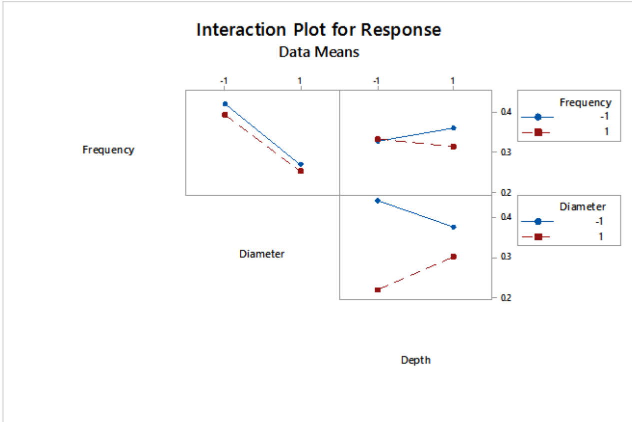

Interaction Plot for Response
Data Means
Frequency
Diameter
Depth
-1
1
0.4
0.3
0.2

(b)

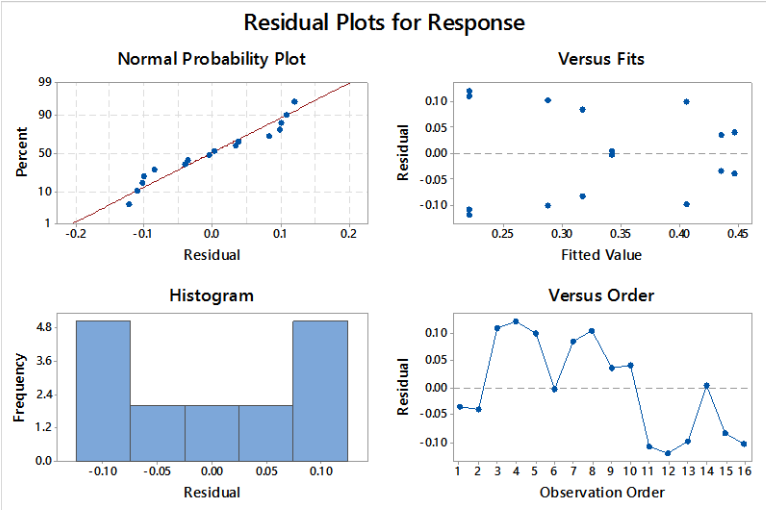

Residual Plots for Response
Normal Probability Plot
Percent
Residual
Versus Fits
Residual
Fitted Value
Histogram
Frequency
Residual
Versus Order
Residual
Observation Order

(c)

Fig. 10

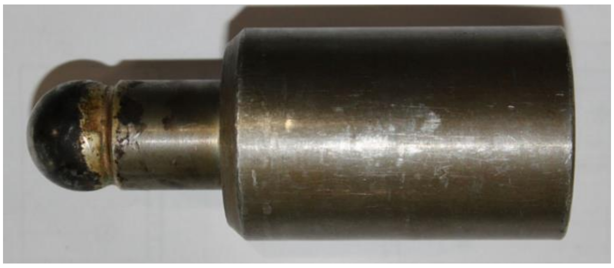

(a)

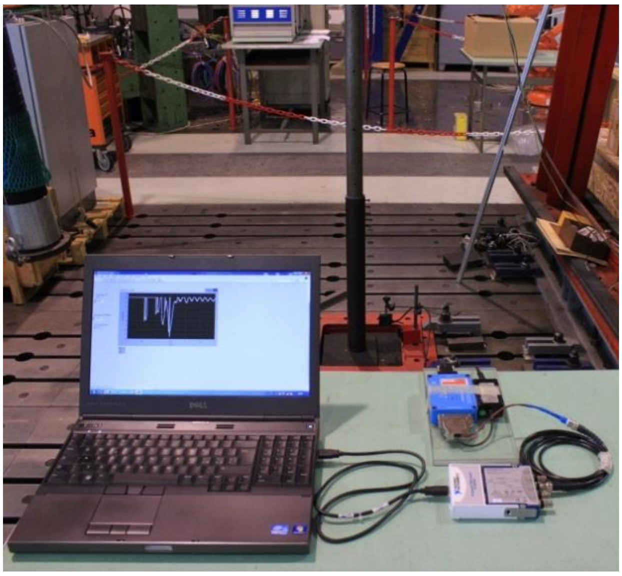

(b)

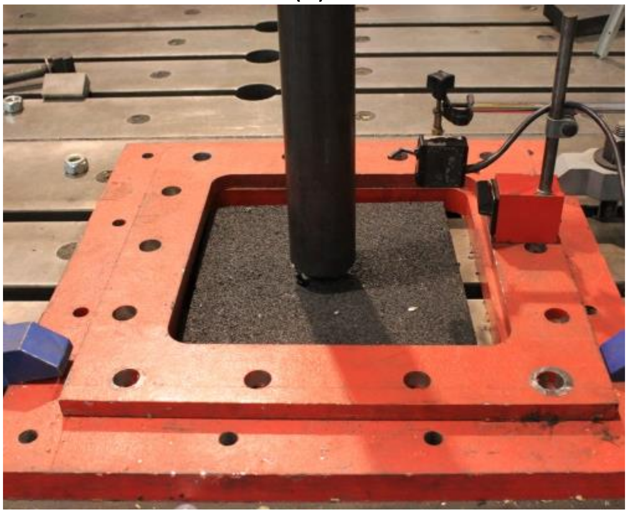

(c)

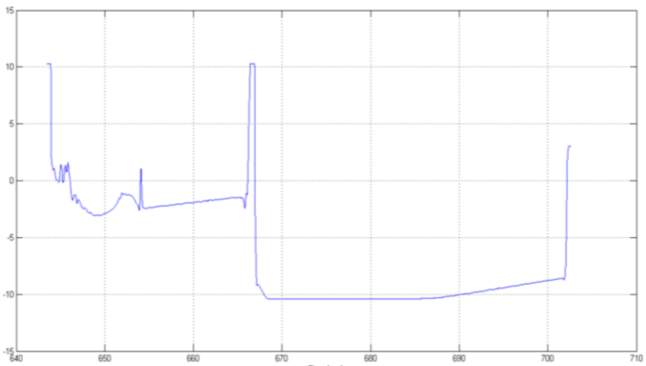

(d)

Fig. 11

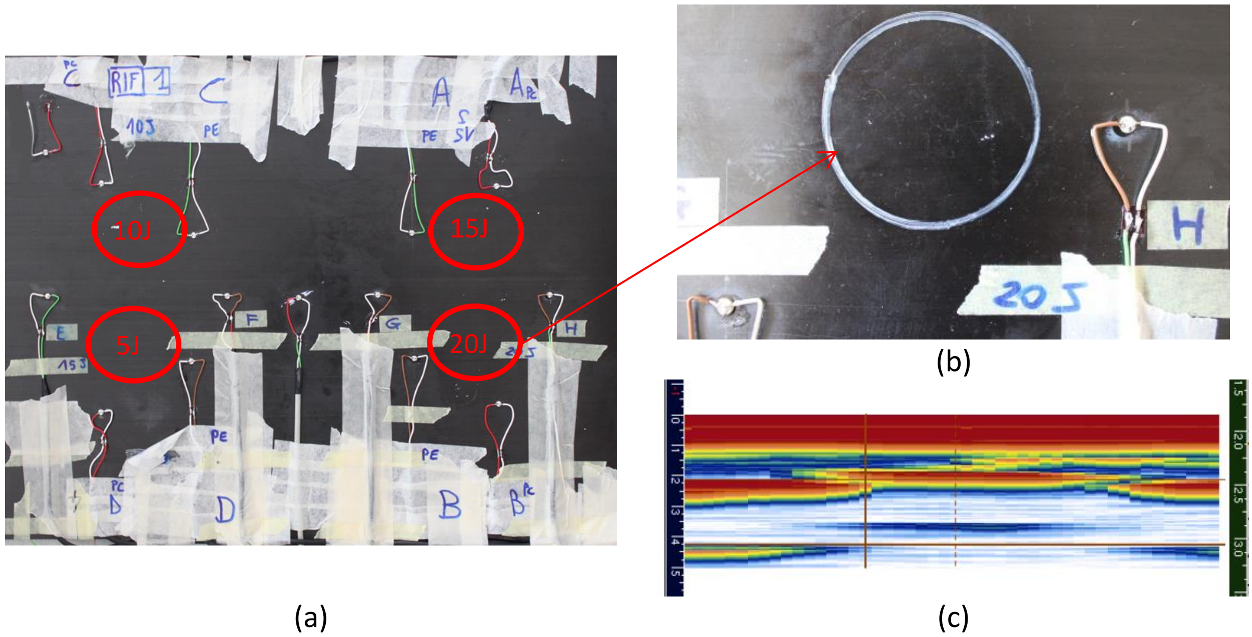

Fig. 12

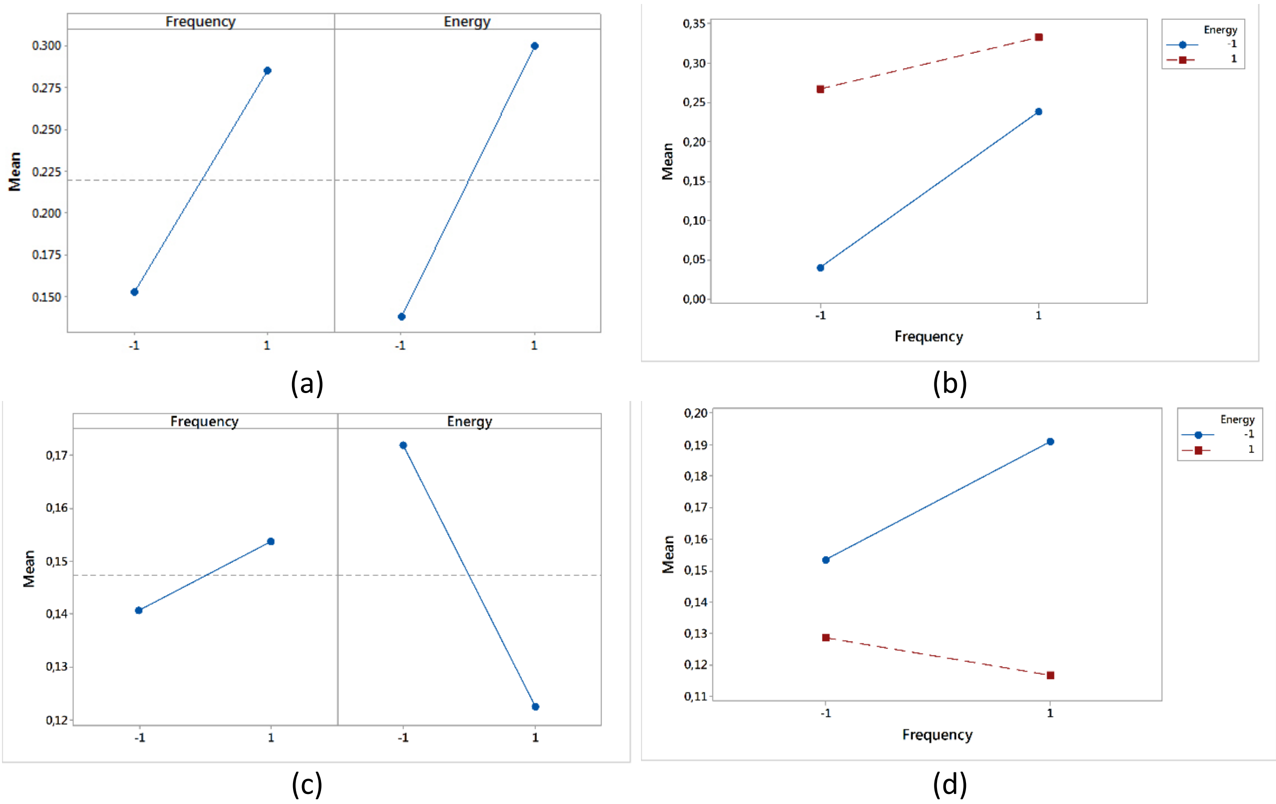
Frequency
Energy
Mean
0.300
0.275
0.250
0.225
0.200
0.175
0.150
-1
1
(a)
Energy
-1
1
0,35
0,30
0,25
0,20
0,15
0,10
0,05
0,00
Mean
Frequency
(b)
Frequency
Energy
Mean
0,17
0,16
0,15
0,14
0,13
0,12
(c)
Energy
0,20
0,19
0,18
0,17
0,16
0,15
0,14
0,13
0,12
0,11
Mean
Frequency
(d)

Fig. 13